Electronic Supplementary Material (ESI) for ChemComm.
This journal is © The Royal Society of Chemistry 2023

Supporting information

The glass transition in the high-density amorphous Zn/Co-ZIF-4

Zijuan Du,[acd] Ang Qiao,[a] Hemin Zhou,[a] Zhencai Li,[b] Wessel M. W. Winters,[b] Jiexin Zhu,[d] Guanjie He,[d] Ivan P. Parkin,[c] Haizheng Tao*[a] and Yuanzheng Yue*[b]

a. State Key Laboratory of Silicate Materials for Architectures, Wuhan University of Technology, Wuhan 430070, China.

b. Department of Chemistry and Bioscience, Aalborg University, DK-9220 Aalborg, Denmark.

c. Christopher Ingold Laboratory, Department of Chemistry, University College London, London WC1H 0AJ, UK.

d. Electrochemical Innovation Lab (EIL), Department of Chemical Engineering, University College London, London WC1E 7JE, UK.

Experimental Synthesis.

All of the chemicals in these experiments were purchased from Shanghai Aladdin Reagent Company and used as received. The synthesis was conducted via a modified solvothermal procedure adapting previously published protocols.[1,2] Specifically, A molar ratio of 1:3.3:1000 for [Zn+Co]: imidazole: N,N-dimethylformamide was used in subsequent experiments. A series of samples, i.e., bimetallic $Zn_{(1-x)}Co_x$-ZIF-4 (where x referred to the nominal molar ratio to be 0, 0.2, 0.4, 0.6, 0.8, 1) were prepared. Firstly, a solid mixture of $Zn(NO_3)_2 \cdot 6H_2O$ and $Co(NO_3)_2 \cdot 6H_2O$ was dissolved in 45 ml of N, N-dimethylformamide (DMF) and vigorously stirred at ambient temperature for 20 minutes to obtain a homogeneous solution. Subsequently, 0.45 g of imidazole (Im) was dissolved into the above solution with continuous stirring for 20 minutes. Afterward, 45 ml of the mixture was tightly sealed in a 100 ml Teflon-lined autoclave, which was heated in an oven at 130 °C for 72 hours for reaction. After cooling to room temperature, the as-obtained precipitates were purified by centrifuging and washing with 15 ml of DMF three times. Finally, the block-shaped crystals of different colors, as depicted in Table 1, were dried at 100 °C for 12 hours.

Table S1. Weight ratios of elements (Zn, Co) and measured molar ratio (R) of Co/(Co+Zn) in the samples measured by ICP-OES.

Sample series	Nominal Co/(Co+Zn) [x]	Zn content (wt%)	Co content (wt%)	Measured Co/(Co+Zn) [R]	Sample formula ($Zn_{1-R}Co_R$-ZIF-4)
bimetallic $Zn_{1-R}Co_R$ ZIF-4 crystals	0.20	26.32	1.47	0.06	$Zn_{0.94}Co_{0.06}(C_3H_3N_2)_2$
	0.40	23.88	3.93	0.15	$Zn_{0.85}Co_{0.15}(C_3H_3N_2)_2$
	0.60	19.22	8.60	0.33	$Zn_{0.67}Co_{0.33}(C_3H_3N_2)_2$
	0.80	11.56	15.02	0.59	$Zn_{0.41}Co_{0.59}(C_3H_3N_2)_2$

Characterizations.

The amounts of Zn and Co in the bimetallic ZIF-4 samples were quantified by the inductively coupled plasma-optical emission spectroscopy (ICP-OES) analysis (Prodigy 7). The powder X-ray diffraction (PXRD) patterns of the ZIF-4 crystal samples were collected by an X-ray diffractometer (D8 Advance) at the 2θ range of 5-40° using Cu K_α (λ=1.540598 Å) radiation. XRD patterns of the high-density amorphous phases (HDAs) were examined by a STOE SEIFERT diffractometer under the radiation source of metal Cu and Mo with detected angular range 2θ of 5°-80° and 2°-40°, respectively. The elemental distributions of the ZIF-4 crystal samples were analyzed by field emission scanning electron microscopy (FESEM, JSM-7610F) equipped with energy dispersive spectroscopy (EDS). The surface morphology and elemental distribution of the HDAs were observed on scanning electron microscopy FEG-SEM JEOL JSM 7600 and transmission electron microscopy (TEM, JEOL JEM-2100). Differential scanning calorimetry (DSC) measurements of the ground samples for ZIF-4 crystals were performed using a DSC instrument (STA449F1, Netzsch) in an argon atmosphere (40 ml min^{-1}) at a rate of 10 °C min^{-1}. All the samples were placed in a platinum crucible situated on a sample holder of the DSC. The HDAs were prepared by heating the crystal to 380 °C at a rate of 10 °C min^{-1}, and then were cooled back to room temperature at 10 °C min^{-1}. The isobaric heat capacity (C_p) curves of the HDAs were recorded at a heating rate of 10 °C min^{-1} through the temperature interval 40-340 °C under flowing argon (40 ml min^{-1}). To determine the the isobaric heat capacity (C_p) curves of the HDA samples, both the baseline (blank) and the reference sample (sapphire) were measured. The fluctuation of the C_p curves is caused by the DSC instrument. Fourier transform infrared (FTIR) absorption spectra in the region of 400-4000

cm^{-1} of HDAs were obtained using a Bruker Model Invenio S FTIR spectrometer at room temperature. Dried samples for analysis were mixed into a potassium bromide (KBr) matrix and pressed into pellets. A Nexus Therno Nicolet spectrometer was utilized to obtain the far-FTIR spectra in the range of 50-600 cm^{-1}. Spectra were obtained with the mixture of paraffin oil and materials placed between thin films of high-density polyethylene. X-ray photoelectron spectroscopy (XPS) measurements were performed by an ESCALAB Xi^{+} X-ray photoelectron spectrometer (Thermo Fischer) using Al Kα radiation. The spectra were calibrated by referencing the binding energy of carbon (C 1s, 284.80 eV).

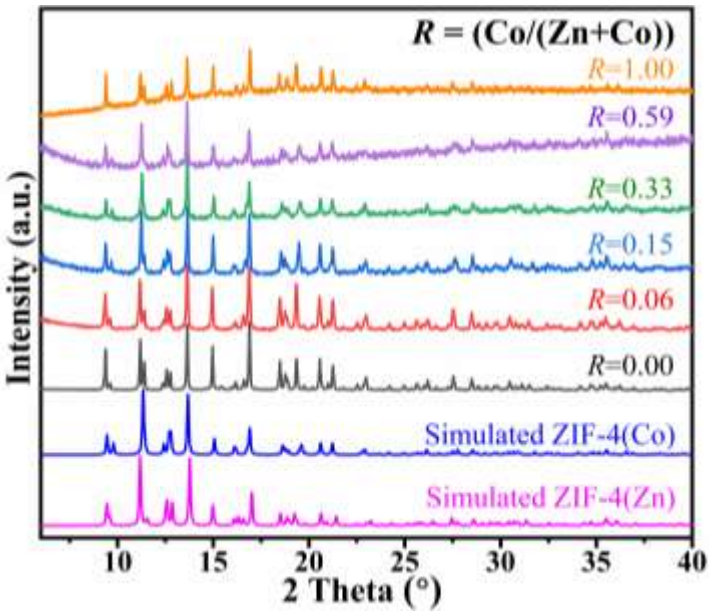

Fig. S1. PXRD patterns of the as-synthesized ZIFs with different experimental molar ratios of *R* (=Co/(Co+Zn)). The patterns have been normalized and offset vertically for clarity.

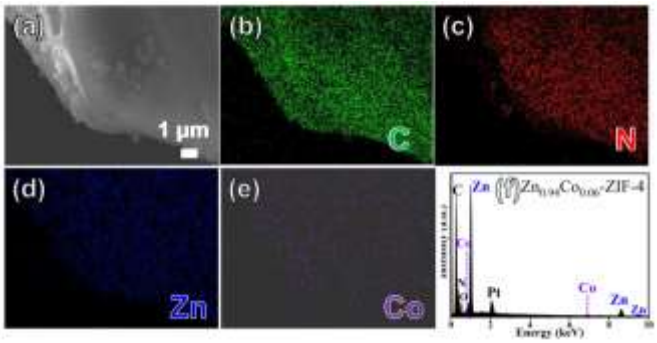

Fig. S2. SEM image (a), elemental mapping analysis (b-e), and EDS spectrum (f) of the bimetallic $Zn_{0.94}Co_{0.06}$-ZIF-4 crystal.

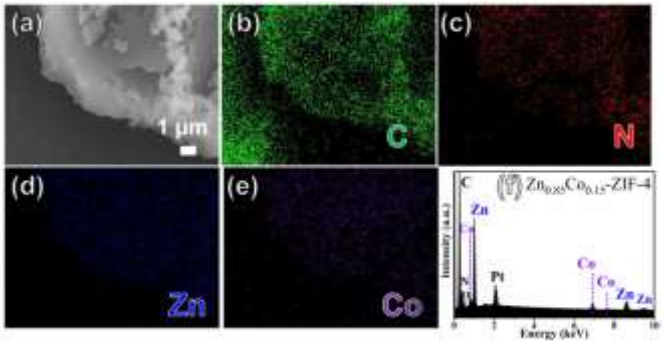

Fig. S3. SEM image (a), elemental mapping analysis (b-e), and EDS analysis (f) of the bimetallic $Zn_{0.85}Co_{0.15}$-ZIF-4 crystal.

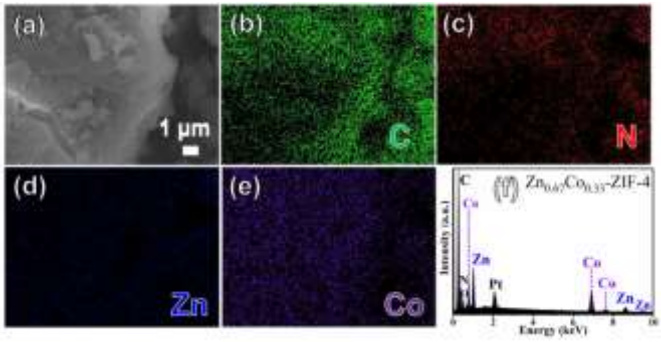

Fig. S4. SEM image (a), elemental mapping analysis (b-e), and EDS analysis (f) of the bimetallic $Zn_{0.67}Co_{0.33}$-ZIF-4 crystal.

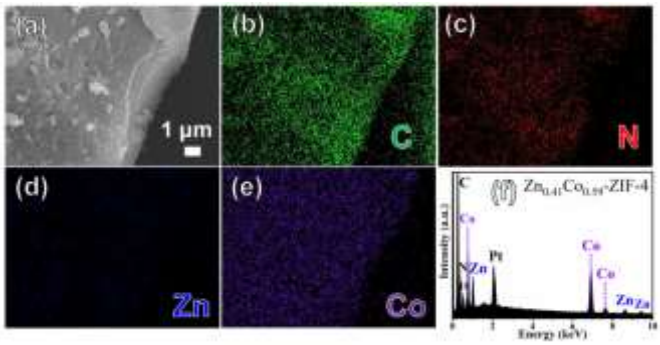

Fig. S5. SEM image (a), elemental mapping analysis (b-e), and EDS analysis (f) of the bimetallic $Zn_{0.41}Co_{0.59}$-ZIF-4 crystal.

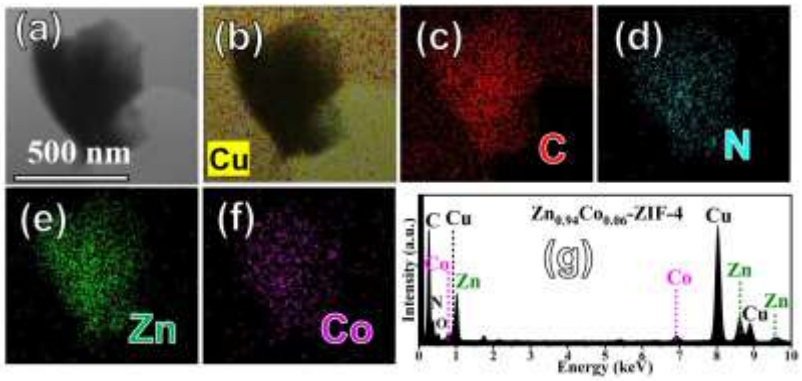

Fig. S6. TEM image (a), elemental mapping analysis (b-f), and EDS spectrum (g) of the bimetallic $Zn_{0.94}Co_{0.06}$-ZIF-4 crystal.

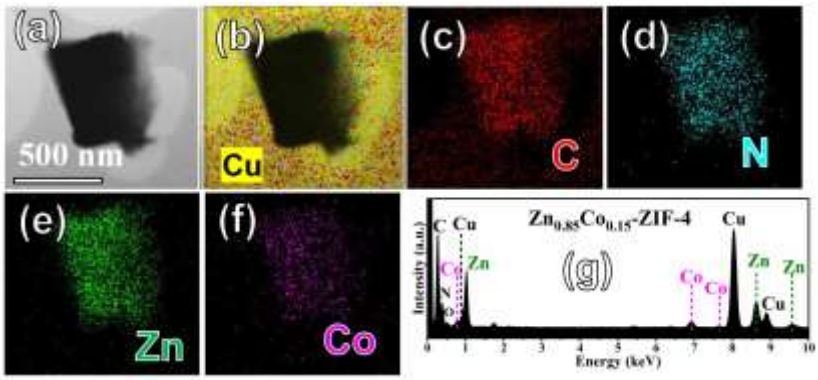

Fig. S7. TEM image (a), elemental mapping analysis (b-f), and EDS spectrum (g) of the bimetallic $Zn_{0.85}Co_{0.15}$-ZIF-4 crystal.

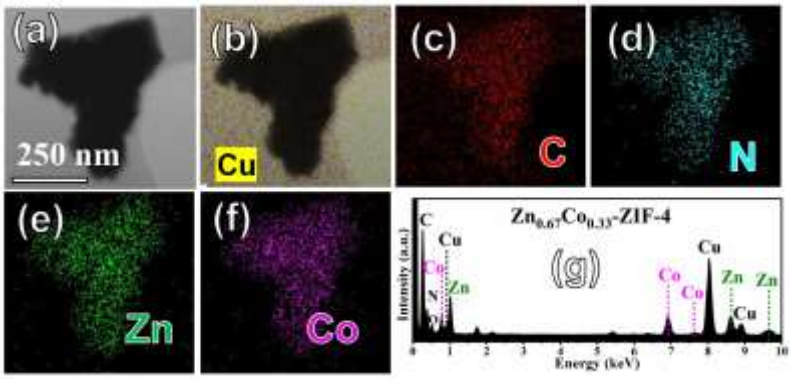

Fig. S8. TEM image (a), elemental mapping analysis (b-f), and EDS spectrum (g) of the bimetallic $Zn_{0.67}Co_{0.33}$-ZIF-4 crystal.

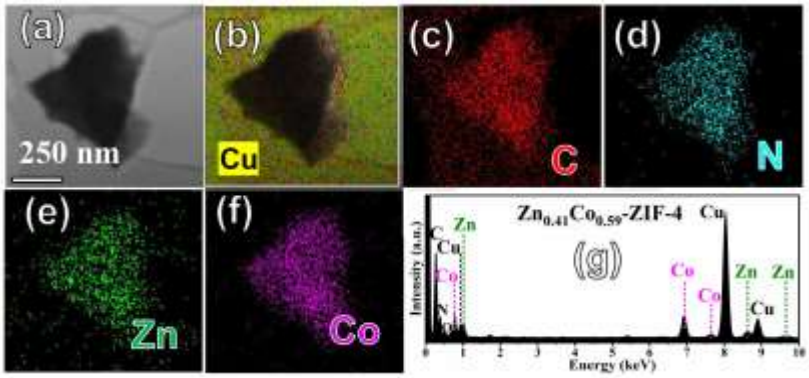

Fig. S9. TEM image (a), elemental mapping analysis (b-f), and EDS spectrum (g) of the bimetallic $Zn_{0.41}Co_{0.59}$-ZIF-4 crystal.

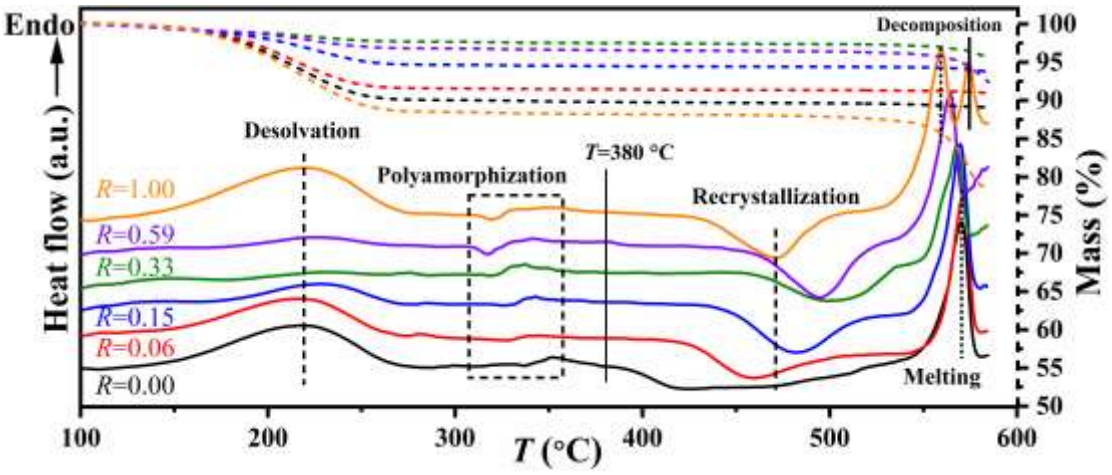

Fig. S10. DSC upscan first curves (solid line) and thermogravimetric analysis (dashed line) in the ZIF-4 crystal samples with different experimental molar ratios (*R*) of Co/(Co+Zn) at a heating rate of 10 °C min^{-1} in argon. The patterns have been normalized and offset vertically for clarity.

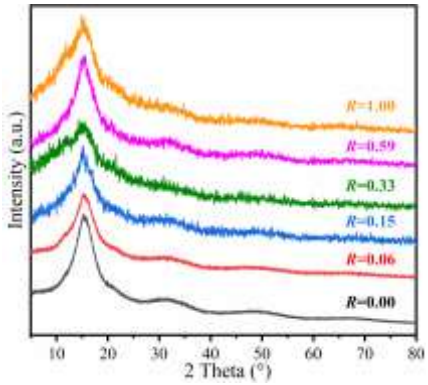

Fig. S11. Powder X-ray diffraction (PXRD) patterns of the as-synthesized $Zn_{1-R}Co_R$-HDA with different experimental molar ratios of *R* (=Co/(Co+Zn)).

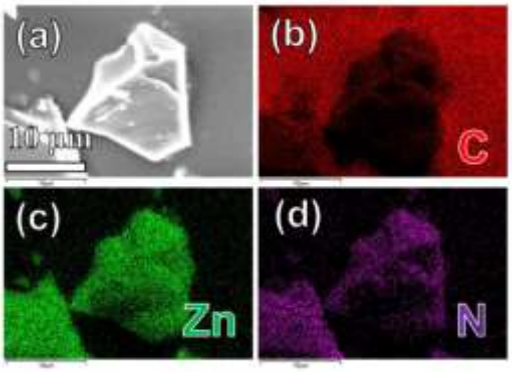

Fig. S12. SEM image (a) and elemental mapping analysis (b-d) of the Zn_1-HDA.

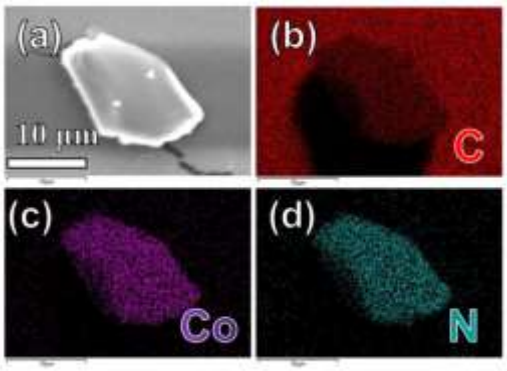

Fig. S13. SEM image (a) and elemental mapping analysis (b-d) of the Co_1-HDA .

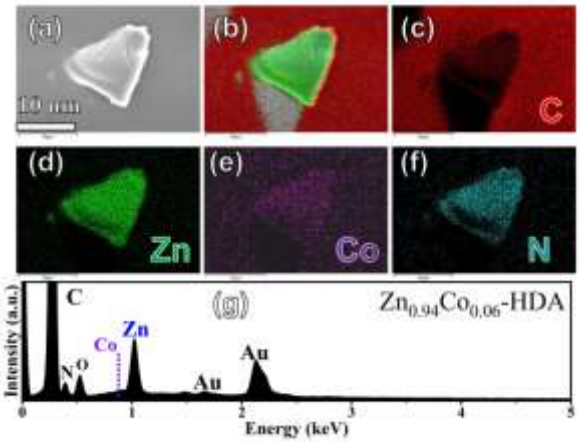

Fig. S14. SEM image (a), elemental mapping analysis (b-f), and EDS spectrum (g) of the bimetallic $Zn_{0.94}Co_{0.06}$-HDA.

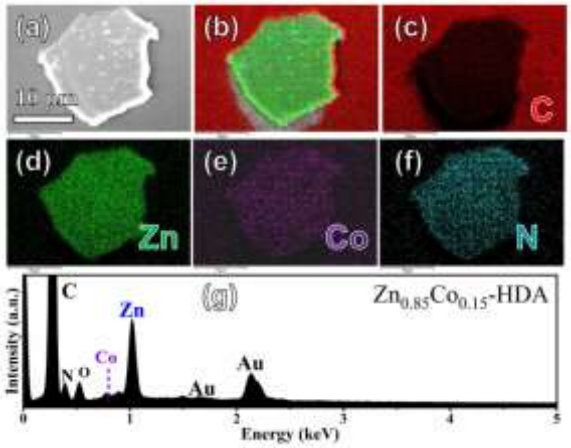

Fig. S15. SEM image (a), elemental mapping analysis (b-f), and EDS spectrum (g) of the bimetallic $Zn_{0.85}Co_{0.15}$-HDA.

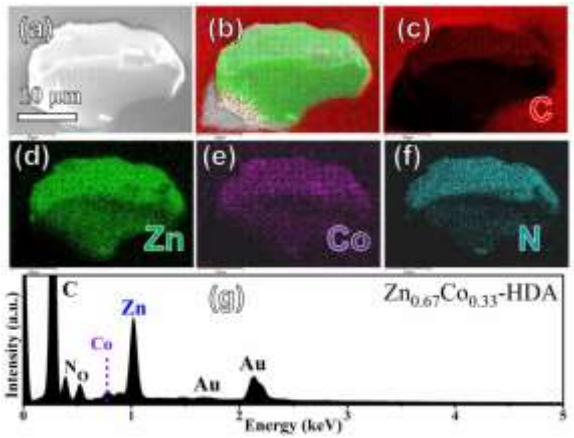

Fig. S16. SEM image (a), elemental mapping analysis (b-f), and EDS spectrum (g) of the bimetallic $Zn_{0.67}Co_{0.33}$-HDA.

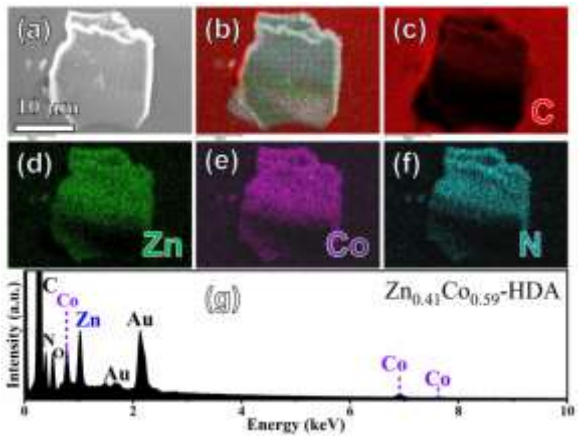

Fig. S17. SEM image (a), elemental mapping analysis (b-f), and EDS spectrum (g) of the bimetallic $Zn_{0.41}Co_{0.59}$-HDA.

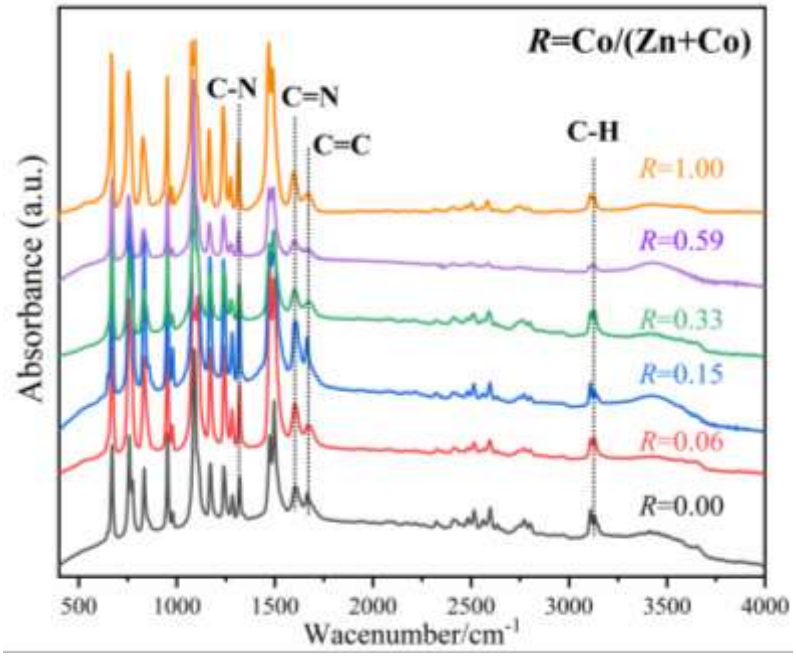

Fig. S18. FTIR absorption curves of high-density amorphous phases (HDAs) in the region 400-4000 cm^{-1}.

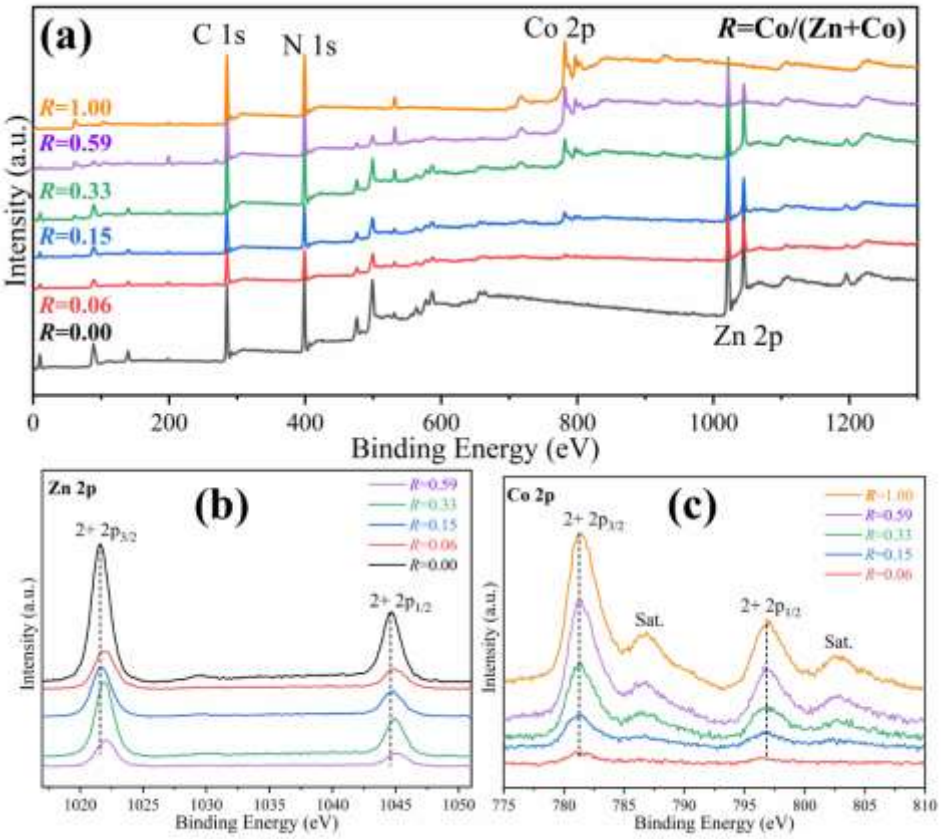

Fig. S19. The wide survey XPS spectra of high-density amorphous phases (HDAs) (a). High-resolution XPS spectra of Zn 2p spectra (b) and Co 2p spectra (c).

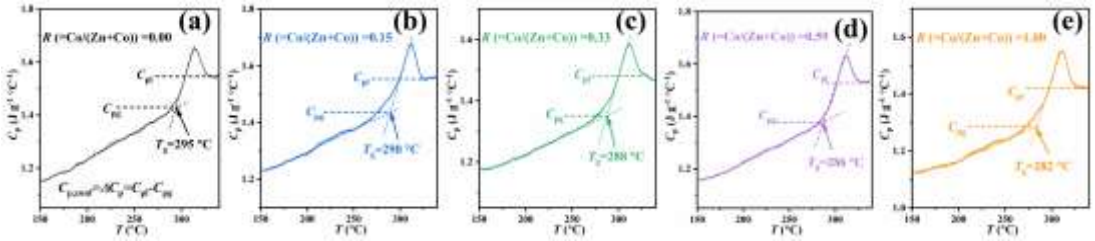

Fig. S20. The isobaric heat capacity (C_p) curves for Zn_1-HDA (a), $Zn_{0.85}Co_{0.15}$-HDA (b), $Zn_{0.67}Co_{0.33}$-HDA (c), $Zn_{0.41}Co_{0.59}$-HDA (d) and Co_1-HDA (e) as measured by DSC under argon gas at a heating rate of 10 °C min^{-1}. The error range of the T_g measurement is ±0.5 °C.

Table S2. The glass transition temperature (T_g) and the calculated configurational heat capacity ($C_{p,conf}$) of high-density amorphous phases (HDAs) with molar ratio R (=Co/(Co+Zn)).

R (=Co/(Co+Zn))	Sample formula of $Zn_{1-R}Co_R$-HDAs	T_g (°C)	$C_{p,conf}$ (J mol^{-1} $°C^{-1}$)
0.00	$Zn_1(C_3H_3N_2)_2$	295	22.35
0.06	$Zn_{0.94}Co_{0.06}(C_3H_3N_2)_2$	292	23.50
0.15	$Zn_{0.85}Co_{0.15}(C_3H_3N_2)_2$	290	24.62
0.33	$Zn_{0.67}Co_{0.33}(C_3H_3N_2)_2$	288	25.86
0.59	$Zn_{0.41}Co_{0.59}(C_3H_3N_2)_2$	286	27.60
1.00	$Co_1(C_3H_3N_2)_2$	282	29.54

References

1 Y. Yu, A. Qiao, A. M. Bumstead, T. D. Bennett, Y. Yue and H. Tao, *Cryst. Growth Des.*, 2020, **20**, 6528-6534.

2 T. D. Bennett, J. C. Tan, Y. Yue, E. Baxter, C. Ducati, N. J. Terrill, H. H. Yeung, Z. Zhou, W. Chen, S. Henke, A. K. Cheetham and G. N. Greaves, *Nat. Commun.*, 2015, **6**, 8079.